Journal of Fluids and Structures (1998) **12,** 153–169

THE INFLUENCE OF UPSTREAM TURBULENCE ON THE STABILITY BOUNDARIES OF A FLEXIBLE TUBE IN A BUNDLE

O. Romberg and K. Popp

Institute of Mechanics, University of Hannover, Appelstrasse 11
30167 Hannover, Germany

(Received 12 August 1996 and in revised form 26 September 1997)

The investigations refer to the influence of isotropic upstream turbulence on the stability behaviour of normal and rotated triangular tube arrays of different pitch-to-diameter ratios. The excitation is due to air cross-flow in a wind tunnel. The experimental apparatus allows the measurement of the stability boundaries of a fully flexible bundle as well as single flexibly mounted tubes with variable equilibrium position in otherwise fixed arrays. By using a turbulence grid with variable geometric properties, it is possible to produce isotropic turbulence with variable turbulence intensity Tu and scale length L_x at the inlet of the bundle. These values were determined using hot-wire anemometers. The investigations show clearly a stabilization with increasing turbulence in case of a single flexibly mounted tube in an otherwise fixed array.

1. INTRODUCTION

Tube failures in heat exchangers are often caused by excessive vibration, especially fluidelastic instability is a dangerous excitation mechanism. In tube arrays subjected to cross-flow, fluidelastic instability has a great potential for short-term damage. Because of the resulting large amplitudes, the onset of this phenomenon must be avoided in any case.

Another excitation mechanism is buffeting, caused by turbulence, which affects the long-term behaviour and also can influence the stability boundaries. The last mentioned effect will be examined in the following.

It has been shown that a flow disturbance *inside the tube array* can change the stability behaviour of a single flexibly mounted tube in the first few rows of an otherwise fixed array in a significant way, cf. Romberg & Popp (1996). There, very thin Prandtl trip-wires were pasted on the surface of the tubes without affecting the flow capacity. Finally, the investigation of the stability behaviour indicated a full suppression of the fluid-damping-controlled instability (galloping) for certain array configurations.

It is a matter of fact that a tube bundle generates turbulence within the first tube rows, cf. Price & Païdoussis (1987) or Sandifer & Baily (1984). A possible explanation for the phenomenon of trip-wire stabilization is an increased level of turbulence and, thus, a disturbance of the flow channels between the tubes, already starting from the first row. The aim of the present study is to investigate experimentally the influence of increased flow turbulence on the stability

0889-9746/98/020153 + 17$25.00/fl970124

boundaries. Here, the increase of turbulence is generated already at the *inlet* of the tube array. The investigation holds for the first four tube rows, where the self-induced turbulence is not fully developed.

To represent the stability behaviour, Connors (1970) introduced a diagram which shows the stability boundaries as a function of the mass-damping parameter $\delta_r = \mu\delta/(\rho d^2)$ and the reduced gap velocity $V_r = U/(f_1 d)$. This standard stability diagram gives a general idea of the stability behaviour of tube arrays in cross-flow which is essential for heat exchanger design. Since a reliable theoretical model is missing, an experimental investigation of the stability boundaries is required. An overview on the stability behaviour of tube bundles subjected to cross-flow by means of Connors diagrams is given by Weaver & Fitzpatrick (1987) and Chen (1984). Fluidelastic instability appears in two different mechanisms: as fluid-damping-controlled instability (galloping) and as fluidelastic-stiffness-controlled instability, cf. Chen (1983).

The galloping mechanism results generally in tube vibrations in the cross-flow direction. For tube excitation, those components of the fluid force are important which are proportional to the tube velocity. In the case of the fluidelastic-stiffness-controlled mechanism, the instability results from coupling effects of several tubes in an array by the fluid. The fluid force terms which depend on the displacement of a tube and its neighbours are decisive. Here, stability investigations require a fully flexible bundle of tubes.

Which of these mechanisms is dominant depends on the configuration of the tube array as well as on the fluid density. Moreover, it is possible that a combination of both effects occurs. In the case of the fluid-damping-controlled instability, the equilibrium position of a single tube becomes unstable. The problem of analysing the stability behaviour of a tube array by investigating only a single flexibly mounted tube in an otherwise fixed row or array is discussed in the literature, cf., e.g. Price & Païdoussis (1986). However, the mechanism of fluid-damping-controlled instability can be *isolated*, using a single flexibly mounted tube in an otherwise fixed array. For certain array configurations, where the galloping mechanism is dominant, the stability boundaries are the same as for a fully flexible bundle. In these cases the stability boundaries of a fully flexible bundle can be determined by the stability of a single flexible tube, cf. Lever & Weaver (1986). In Austermann & Popp (1995) a comparison of the stability boundaries of a single flexibly mounted tube with that of a fully flexible bundle can be found. For the tube configuration investigated here, the agreement for the lower and decisive stability boundary is very good.

The experimentally determined stability boundaries for small upstream turbulence intensity (laminar flow) in a wind tunnel are well known, cf., e.g. Austermann & Popp (1995). The phenomenon of primary damages in the first few rows leads also to the question of the influence of upstream turbulence on the stability behaviour of the tubes. Soper (1982) observed an influence of grid-generated turbulence on the stability behaviour of tube bundles in cross-flow. Also, Southworth & Zdravkovich (1975) and Gross (1975) found that turbulence completely changes the fluid elastic response of in-line tube banks. The effect of the generated turbulence on the tube bundle stability is contradictory in the literature. Gorman (1979) reaches the conclusion that upstream generated turbulence using grids and screens can suppress high amplitudes of tubes in a bundle. He hypothesizes that a grid breaks up the longitudinal correlation of fluid forces acting on flexible tubes. On the contrary, Rzentkowski & Lever (1995) investigated this problem theoretically based on a nonlinear model; they found that turbulence can trigger fluidelastic instability in the case of unstable bifurcations.

2. DESCRIPTION OF TURBULENCE

According to a classification by Rotta (1972), turbulent flow is an irregular three-dimensional eddy flow. The three-dimensional velocity distribution $\mathbf{u}$ of a flow fluid can be described as the sum of the mean velocity $\bar{\mathbf{u}}$ and a disturbance velocity $\mathbf{u}'$. One component can be expressed as

$$u_i(\mathbf{x}, \mathrm{t}) = \overline{u_i}(\mathbf{x}, t) + u_i'(\mathbf{x}, t). \tag{1}$$

In the present study, the special case of wind-tunnel turbulence is considered. Here, with a screen in front of a nozzle, the flow is calmed and rectified before it reaches the test-section. The turbulence can be considered as homogeneous and spatially independent (isotropic). More details can be found in Batchelor (1953) and Rotta (1972).

Under the assumption of a stationary ergodic Gaussian velocity process u_i, it is possible to describe the turbulence in the test-section of a wind tunnel by the mean,

$$\overline{u_i}(\mathbf{x}) = \lim_{T\to\infty} \int_{-T}^{T} u_i(\mathbf{x}, t)\,\mathrm{d}t, \tag{2}$$

and the variance,

$$\sigma_i^2(\mathbf{x}) = \overline{u_i'^2}(\mathbf{x}) = \lim_{T\to\infty} \int_{-T}^{T} [u_i(\mathbf{x}, t) - \overline{u_i}(\mathbf{x})]^2\,\mathrm{d}t. \tag{3}$$

These quantities provide the turbulence intensity Tu,

$$\mathrm{Tu} = \frac{\sigma_1}{\overline{u_1}}, \tag{4}$$

where the index "1" describes the in-flow direction, x.

Another parameter which specifies the spatial character of the flow field is the length scale L. We consider the correlation function.

$$R_{ij}(\mathbf{x}, t, \mathbf{r}, \tau) = \overline{u_i'(\mathbf{x}, t) u_j'(\mathbf{x}^*, t^*)}, \tag{5}$$

where $r = \mathbf{x}^* - \mathbf{x}$ is the correlation width and $\tau = t^* - t$ is the correlation time. In this general form, R_{ij} describes all space- and time-dependent correlations of the velocity components. The length scale is defined as

$$L_{ij,k} = \frac{1}{\overline{u_i'(\mathbf{x}, t) u_j'(\mathbf{x}, t)}} \int_0^{\infty} R_{ij}(\mathbf{x}, t, r_k, 0)\,\mathrm{d}r_k. \tag{6}$$

To describe the spatial character of isotropic grid turbulence the length scale L_x, calculated by the autocorrelation function $R_{11}(\tau)$, is considered. The autocorrelation function can be described with sufficient accuracy by

$$\frac{R_{11}(\tau)}{\sigma_1^2} = \exp\left(-\frac{U_\infty |\tau|}{L_x}\right), \tag{7}$$

cf. Fung (1968). Here, U_∞ is the undisturbed upstream velocity, $U_\infty = \overline{u_1}$. Due to the Taylor hypothesis (1938) of "frozen turbulence", this yields immediately the length scale L_x, without using equation (6). Experimental investigations verify this relation, which can be found, for example, in Lindner (1993). The parameter L_x characterizes an area with noticeably

correlated velocities and can be understood as the average length of a turbulence eddy. With respect to the stability investigations in this study, the reduced length scale

$$L_{x,\mathrm{red}} = L_x/d \tag{8}$$

is introduced, where d is the tube diameter.

3. GENERATION OF UPSTREAM TURBULENCE

The experimental investigations were carried out in both apparatuses used by Andjelić & Popp (1989), as well as Austermann & Popp (1995). The arrays consist of aluminium tubes with an outside diameter of $d = 80\,\mathrm{mm}$ and a length of $l = 800\,\mathrm{mm}$. The arrays are mounted within the test-section of a wind tunnel. The side walls of the test-section allow to realize different tube patterns which are usual in heat exchangers: e.g., normal and rotated triangular arrays, see Figure 1. With respect to the rotated triangular array, one flexibly mounted tube in an otherwise fixed tube bundle has been investigated, since it characterizes the stability of the fully flexible array (Austermann & Popp 1995). It is possible to vary the row number, equilibrium position and damping of the tube. The tested rotated triangular tube array with $P/d = 1{\cdot}375$ consists of six rows of 15 cylinders altogether and six half-tubes, as shown in Figure 2.

As a matter of fact, the stability boundaries for a fully flexible normal triangular bundle are not in accordance with those of a flexibly mounted tube within a fixed array (Austermann & Popp 1995). Therefore, the investigations for the normal triangular array with ($P/d = 1{\cdot}25$) are carried out with a fully flexible bundle of 18 flexibly mounted tubes, where nine of them have variable damping and linear iso-viscoelastic mounting. The tube motions in both apparatuses have been determined by a set of strain gauges, cf. Andjelić & Popp (1989) and Austermann & Popp (1995). The turbulence intensity of the free upstream flow is about $\mathrm{Tu} = 1\%$. To determine the relation between the upstream velocity U_∞ and the gap velocity U, we have to look at the basic array configurations shown in Figure 1. Applying the continuity equation for the normal triangular array yields

$$U = U_\infty P/(P - d). \tag{9}$$

For a rotated pattern the relation

$$U = U_\infty P \sin\alpha/(P - d) \tag{10}$$

is used, where α denotes the flow angle, see Figure 1.

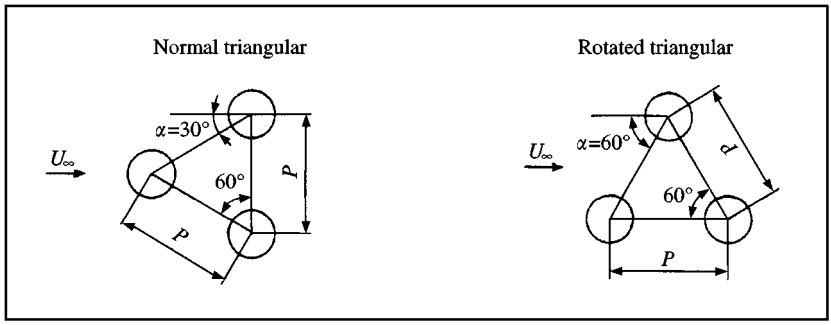

Figure 1. Heat exchanger tube configurations investigated here.

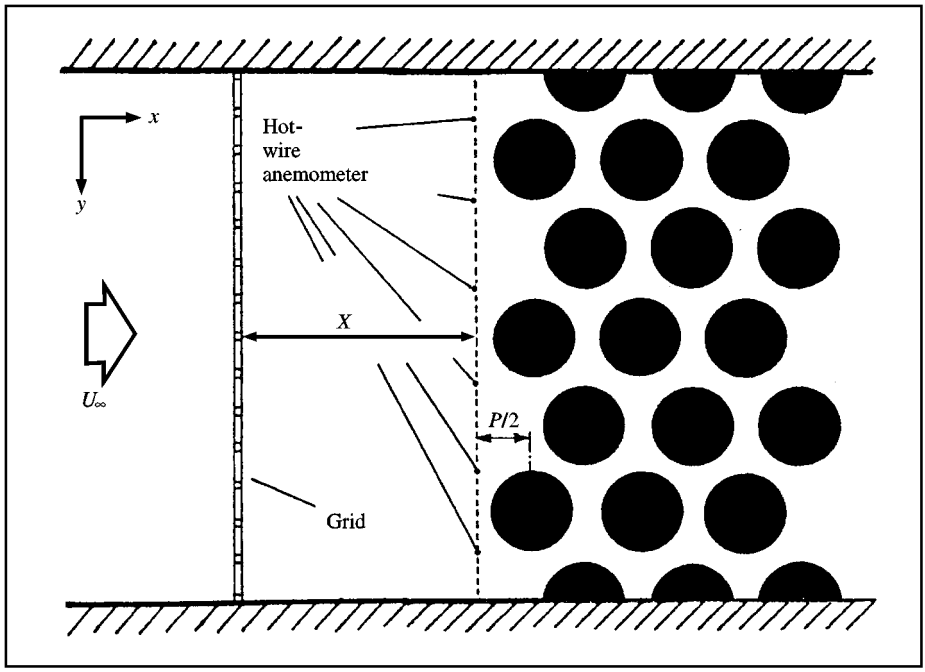

Figure 2. Experimental set-up for increasing the turbulence at the inlet of the tube bundle.

To vary the turbulence field in the test-section of a wind tunnel, turbulence grids are generally used. Here, the grid is placed in front of the tube array at a specific but variable distance X, see Figure 2. Figure 3 shows a photograph of the experimental set-up where on the left-hand side one of the grids made of wood can be seen. The grid distance X is defined as the distance between the grid and the inlet of the bundle. In this study, the inlet is the plane in a distance b in front of the mid-point of the first row. The distance b was chosen to $b = P/2$ for the rotated triangular array and to $b = \sqrt{3}P/2$ for the normal triangular array.

Figure 4 shows the geometry of the grid. The flow separates at the bars of the grid and merges behind them. This yields a broad-band turbulence distribution. The turbulence has been measured by a hot-wire anemometer. The hot wire was placed at 24 points vertical to the flow at the inlet of the tube array, see Figure 2. The outer points of the measured field were located 50 mm in the y-direction and 100 mm in the z-direction away from the wall of the test-section to avoid undesired effects caused by the boundary layer. In the following, the measured fluid velocity is called u_1.

The turbulence behaviour of the flow behind a grid has been investigated by many authors. For example, Baines & Peterson (1951) showed that for grids and screens homogeneous flow is obtained at a distance of 20 bar widths behind a turbulence grid. At this distance, maximum turbulence intensity Tu can be observed. The relation between the surface areas of the grid bars and the grid meshes must be smaller than 50%. With increasing grid distance X, the turbulence intensity Tu decreases and the length scale L_x grows. The experimental investigations in this study show a good agreement with the theoretical considerations of the decay of turbulence by Frenkiel (1948).

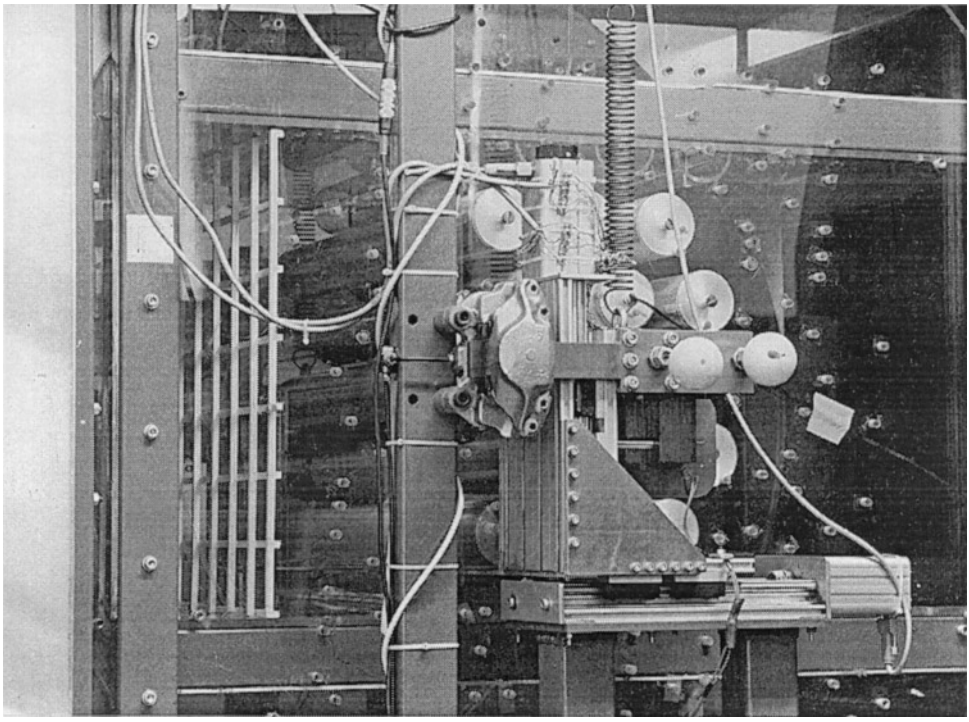

Figure 3. Test array with mounted turbulence grid in front of the tube bundle.

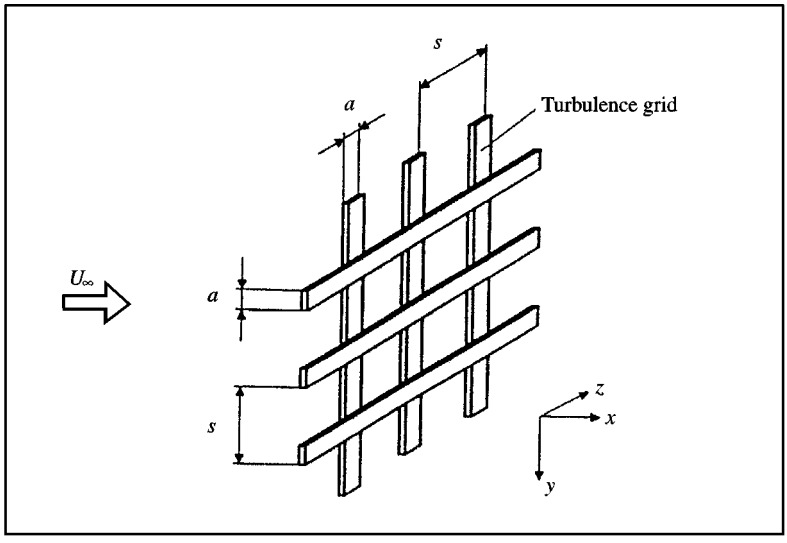

Figure 4. Section of a turbulence grid which is placed in front of the tube bundle to realize homogeneous upstream turbulence.

In a first step, the probability density distribution of the generated turbulence in the test-section has been investigated. Figure 5 shows the distribution of 4096 values of the velocity fluctuation u'_1 for a certain grid configuration. The calculated normal distribution is in good agreement with the measured points. Here, a possible dependence of the turbulence on the fluid velocity U_∞ has to be considered. However, Figure 6 shows that the influence of the fluid velocity U_∞ or reduced gap velocity V_r on the turbulence intensity Tu can be neglected. Secondly, the grid distance X, the mesh size s, the bar width a, the geometry of the bars and the tube bundle itself have an influence on the turbulence intensity Tu and the length scale L_x.

Table 1 shows the grid configurations used in this study. For rotated triangular tube arrays, grid configurations R1, R2 and R3 with various reduced distances $X_{\text{red}} = X/a$ have been implemented, see Table 2. This table shows the determined values of Tu and L_x. For the normal triangular tube array the grid configurations N1, N2 and N3 are used. The distances investigated with the corresponding turbulence values are given in Table 3. Furthermore, the following symbols are used for the two different array configurations: $\triangle$: rotated triangular array; $\triangleright$: normal triangular array.

Figure 7 shows the field of turbulence intensity Tu at the inlet of the rotated triangular tube array with a pitch to diameter ratio of $P/d = 1{\cdot}375$ without a turbulence grid (Tu = 3·5%, $L_{x,\text{red}} = 0{\cdot}39$). The turbulence parameters for a certain grid configuration are defined by the average values of all 24 points of the field mentioned above. The turbulence distribution, e.g. for grid configuration R1 and a reduced grid distance $X_{\text{red}} = 32{\cdot}5$, cf. Table 2, is shown in Figure 8. It can be seen that the turbulence intensity Tu is homogeneous and larger than without the grid.

The investigations confirm the fact that increasing the grid distance X reduces the turbulence intensity. The measurements in Figures 9 and 10 show satisfactory agreement

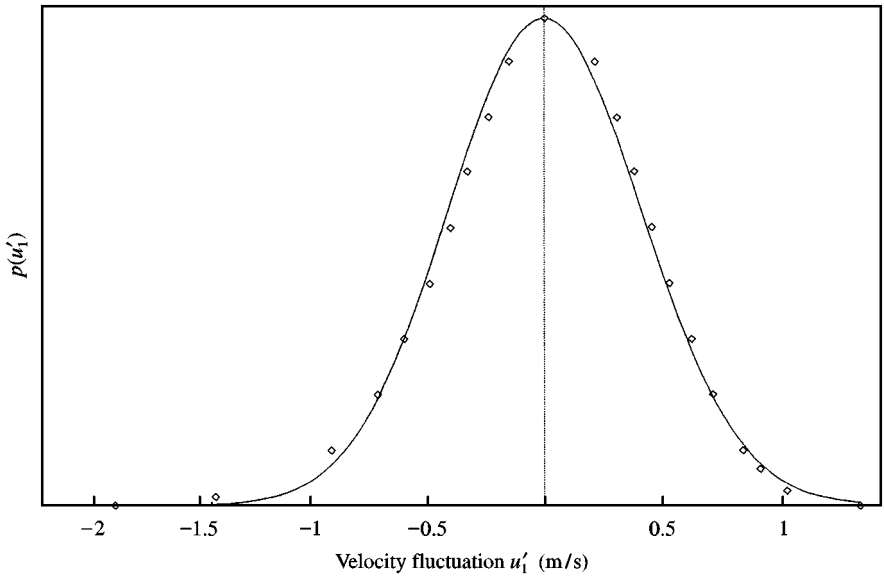

Figure 5. Comparison of the measured fluid velocity distribution behind the turbulence grid R2 (○) with the calculated normal distribution, $p(u'_1) = [1/\sqrt{2\pi\sigma_i^2}]\exp(-u_1'^2/2\sigma_1^2)$, $\sigma_1 = 0{\cdot}42$.

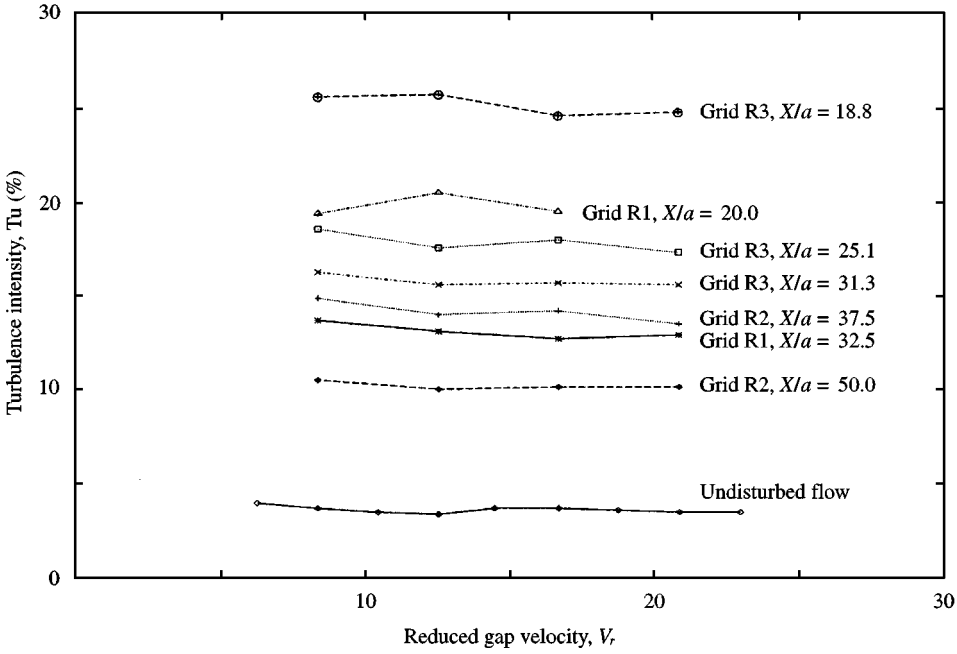

Figure 6. Measured turbulence intensity Tu as a function of the reduced gap velocity V_r for several grid configurations.

TABLE 1
Grid configurations used in this study

Notation	Bar width, a (mm)	Mesh size, s (mm)
	Rotated triangular array	
Grid R1	8	40
Grid R2	8	80
Grid R3	16	80
	Normal triangular array	
Grid N1	7	50
Grid N2	7	100
Grid N3	14	100

TABLE 2
Turbulence parameters for the rotated triangular array

	X_{red}		20	32·5	45
Grid R1	Tu		19·7%	13·4%	10·5%
	$L_{x,red}$		0·25	0·26	0·29
	X_{red}	22·5	27·5	37·5	50
GridR2	Tu	13·8%	13·8%	11·9%	10·1%
	$L_{x,red}$	0·21	0·23	0·26	0·29
	X_{red}		18·75	25	31·25
GridR3	Tu		23·0%	18·3%	14·7%
	$L_{x,red}$		0·26	0·29	0·33

TABLE 3
Turbulence parameters for the normal triangular array

	X_{red}	28·6	42·9	57·1
Grid N1	Tu	16·5%	14·5%	11·6%
	$L_{x,red}$	0·25	0·34	0·38
	X_{red}	28·6		57·1
Grid N2	Tu	11·3%		10·9%
	$L_{x,red}$	0·24		0·34
	X_{red}		21·4	28·6
Grid N3	Tu		21·1%	16·8%
	$L_{x,red}$		0·28	0·3

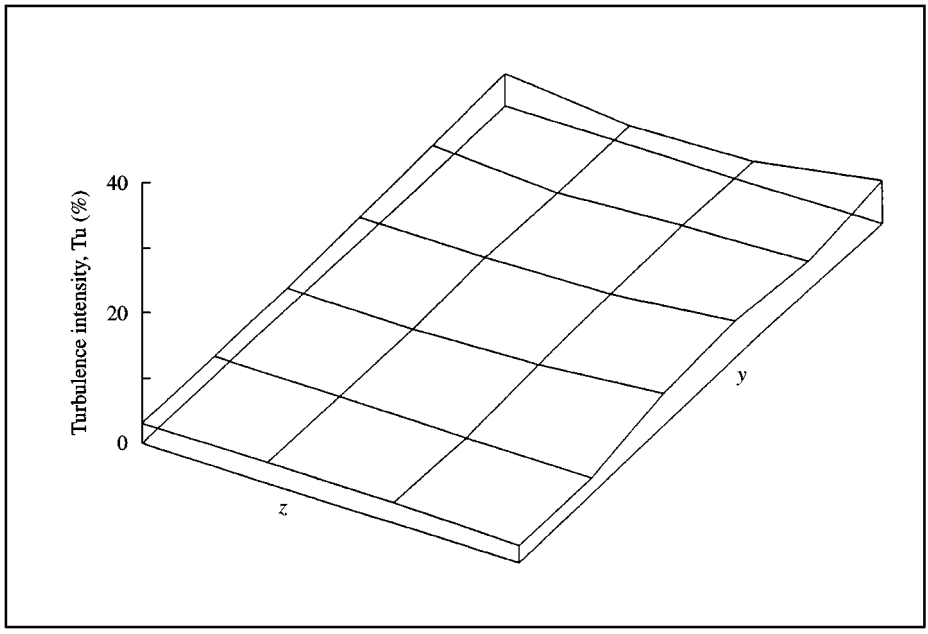

Figure 7. Measured turbulence intensity Tu in a field of 24 points at the inlet of the tube bundle without turbulence grid.

with the turbulence decay given by Frenkiel (1948). The length scales L_x have been determined from the measured autocorrelation function using equation (7). Figure 11 shows the comparison of the measured and calculated autocorrelation function for the grid configuration N1. The value L_x determined for all grids considered and tube bundle configurations can be found in Tables 2 and 3.

4. INFLUENCE ON THE STABILITY BEHAVIOUR

A reliable determination of stability boundaries demands the exact knowledge of the vibration behaviour of the system considered and requires a stability criterion (Chen 1988). In this study, the amplitude criterion used also by Austermann & Popp (1995) has been

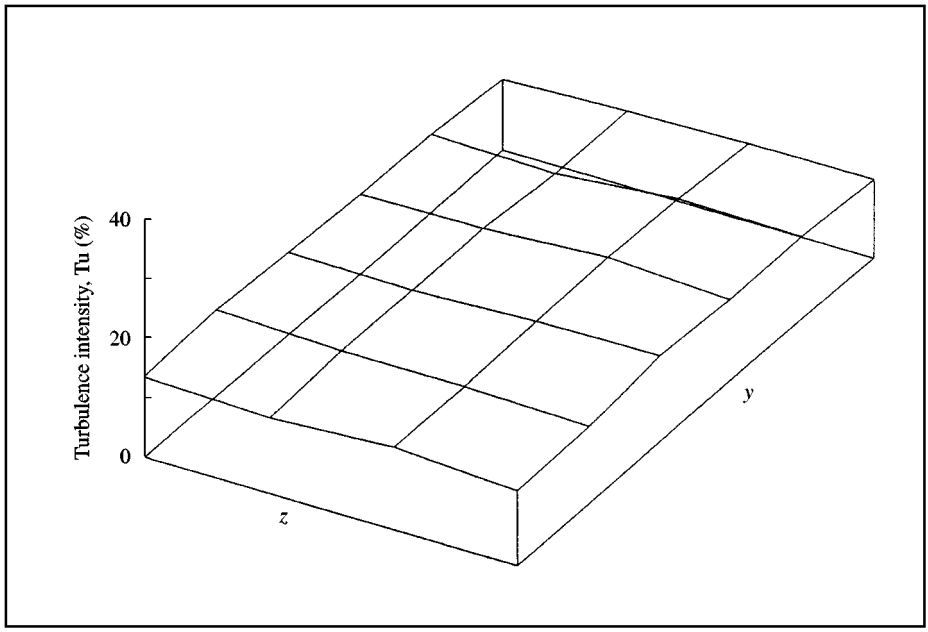

Figure 8. Measured turbulence intensity Tu in a field of 24 points at the inlet of the tube bundle for grid configuration R1.

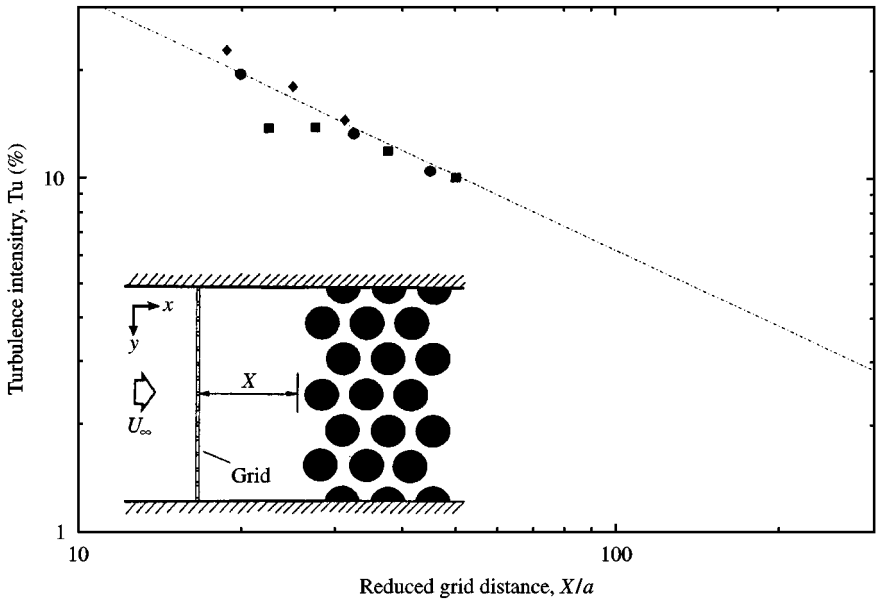

Figure 9. Dependence of the turbulence intensity Tu on the grid distance X for the rotated triangular configuration: ●, grid R1; ■, grid R2; , ◆, grid R3; - - -, calculated.

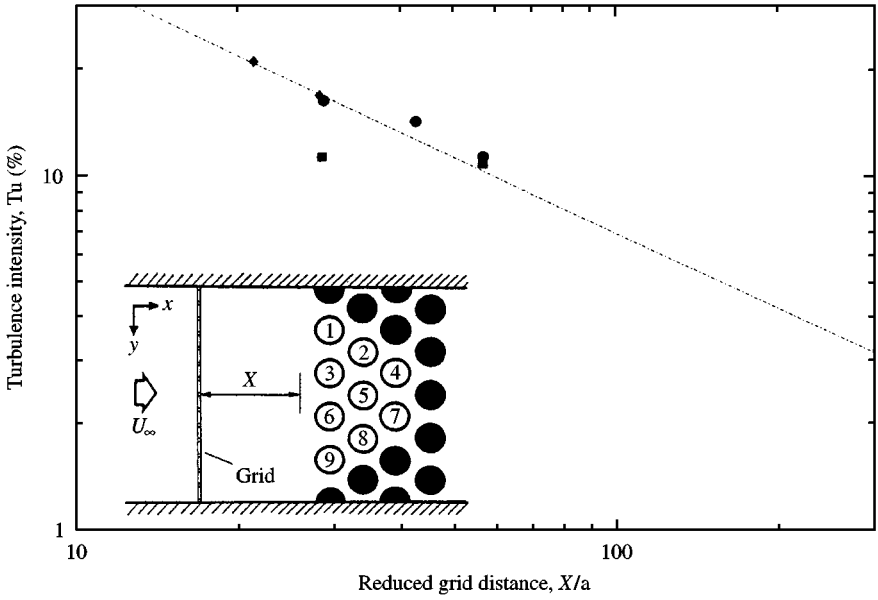

Figure 10. Dependence of the turbulence intensity Tu on the grid distance X for the normal triangular configuration: ●, grid N1; ■, grid N2; ◆, grid N3; - · - , calculated.

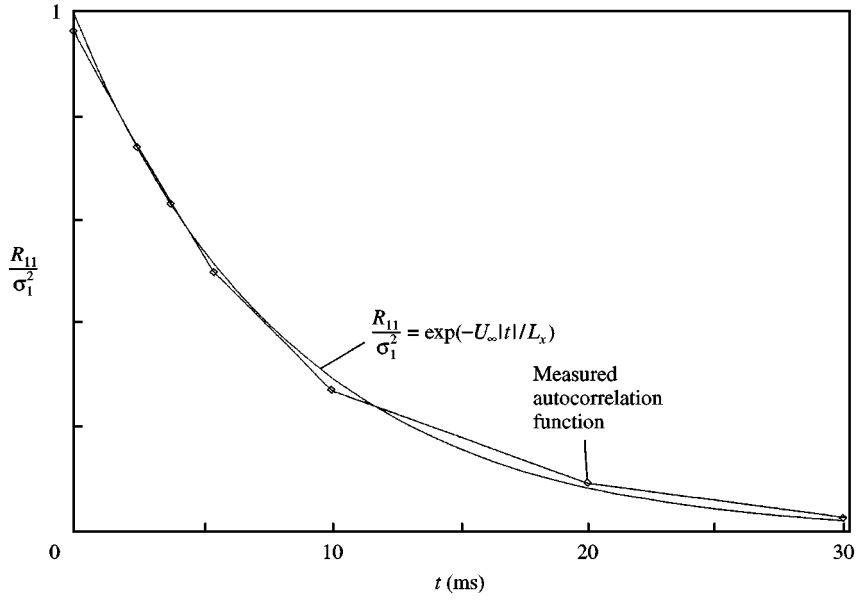

Figure 11. Determination of the length scale L_x from the measured auto-correlation function; $a = 7$, $s = 50$, $x = 300$; $L_x = 27$ mm.

applied. The stability is investigated considering the amplitude behaviour depending on the reduced gap velocity V_r for a fixed mass-damping parameter δ_r. A sudden change to large amplitudes in the cross-flow direction characterizes the stability boundary. For more details see Austermann & Popp (1995).

4.1. Rotated Triangular Array ($P/d = 1{\cdot}375$)

Figure 12 shows the measured reduced amplitude as a function of the reduced gap velocity V_r and the mass-damping parameter δ_r for a single flexibly mounted tube in the critical third row of an otherwise fixed array with ideal geometry.

In the critical third row, not only do the largest amplitudes occur, but also the smallest values of the critical reduced gap velocity are found; see Austermann & Popp (1995) and Figure 14. The investigations are limited to arrays with an ideal geometry, which is most sensitive to fluidelastic instability.

In the stable region the tube moves with small amplitudes in the cross- and in-flow directions due to turbulent buffeting. In the unstable mode the tube executes galloping motions exclusively in the cross-flow direction. To protect the experimental set-up, the measurements have to be stopped if the tube reaches a reduced amplitude of about 12%.

Figure 13 shows the amplitude as a function of the reduced gap velocity V_r and the mass-damping parameter δ_r for the critical third row, similarly to Figure 12, but for increased turbulence. Here, the lowest grid-generated turbulence intensity ($\mathrm{Tu} = 10{\cdot}1\%$, $L_{x,\mathrm{red}} = 0{\cdot}29$) is adjusted, see Table 2. The significant stabilization due to turbulence can easily be seen. This effect appears also for other selected grid configurations, i.e. for larger turbulence intensities. There is no predominance of the fluid-damping-controlled excitation mechanism anymore.

The investigations have been carried out at the first four rows of the tube array. The stability diagram for the first rows can be seen in Figure 14 [presented by Austermann & Popp (1995)].

Figure 15 shows the stability diagram for the same array configuration considered in Figure 14, but with increased turbulence. For very small values of the mass-damping

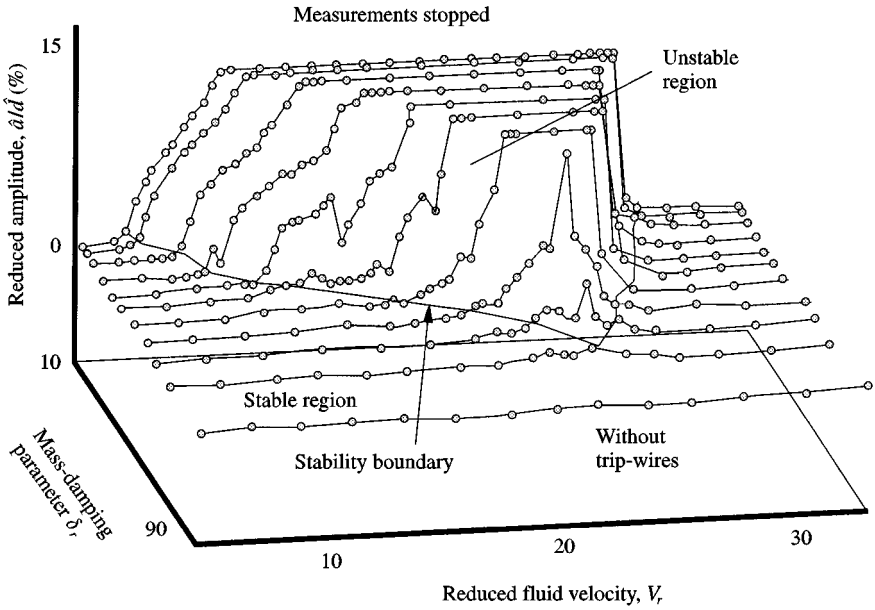

Figure 12. Measured reduced amplitudes as a function of V_r and δ_r for a single flexibly mounted tube in the critical third row of an otherwise fixed array.

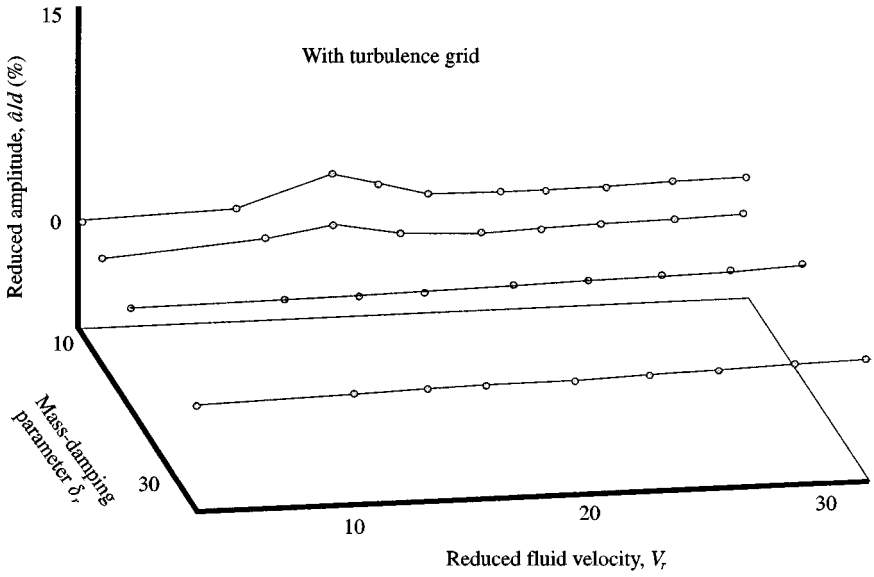

Figure 13. Measured reduced amplitudes as a function of V_r and δ_r for a single flexibly mounted tube in the critical third row of an otherwise fixed array with increased turbulence (grid R2, Tu = 10·1, $L_{x,\mathrm{red}} = 0{\cdot}29$).

parameter δ_r, the first as well as the third row become unstable. The stability boundaries of the second and fourth rows disappear for the ideal array geometry. Here, the stability investigations with respect to increased turbulence yield exclusively small amplitudes due to turbulence excitation.

4.2. Normal Triangular Array ($P/d = 1{\cdot}25$)

For the normal triangular array there is not sufficient agreement between the stability behaviour of a single flexibly mounted tube in an otherwise fixed array and the stability boundary of a fully flexible bundle of the same geometry. For this array configuration it is generally accepted that the fluid-damping-controlled mechanism is not the predominant one. Thus, investigations for this configuration have been carried out using the fully flexible bundle used also by Andjelić & Popp (1989). Nine of these tubes (see Figure 16) are equipped with linear iso-viscoelastic tube mountings and variable damping. The amplitude criterion mentioned is applied to any flexibly mounted tube that becomes unstable. The stability boundary for undisturbed flow (Tu = 5·4%, $L_x = 0{\cdot}38$) coincides with that measured by Andjelić & Popp (1989). The investigations with increased turbulence were carried out with three different grid configurations, see Table 3. Note, that for this array configuration the turbulence intensity Tu at the inlet of the array is quite large (Tu = 5·4%) . Thus, the influence of the grid-generated turbulence compared with the array-induced turbulence probably is small for this array configuration.

Figure 16 shows that for small mass-damping parameters δ_r and increasing turbulence intensity Tu there seems to be a small influence on the stability boundary, i.e. a slight shift to higher reduced gap velocities V_r. However, the differences of the stability threshold estimation are nearly within the range of the measurement error.

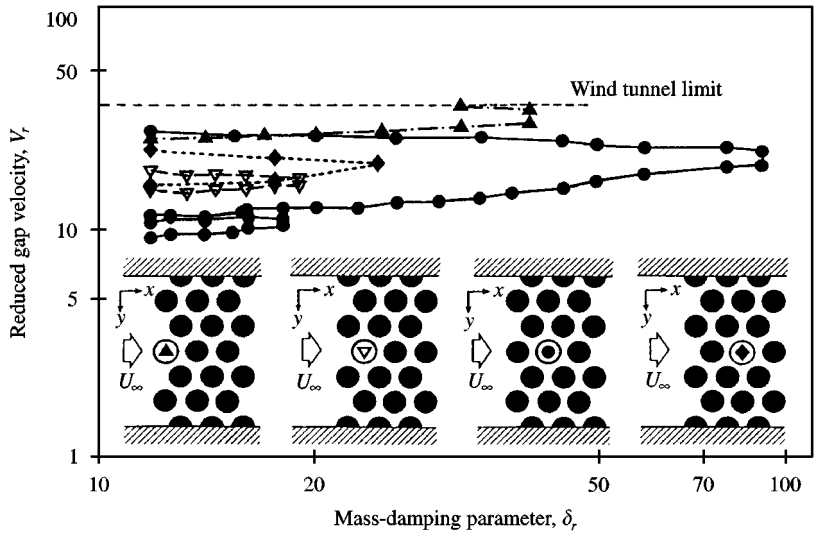

Figure 14. Stability diagram for a flexibly mounted tube in different locations in an otherwise fixed rotated triangular array ($P/d = 1{\cdot}375$), from Austermann & Popp (1995).

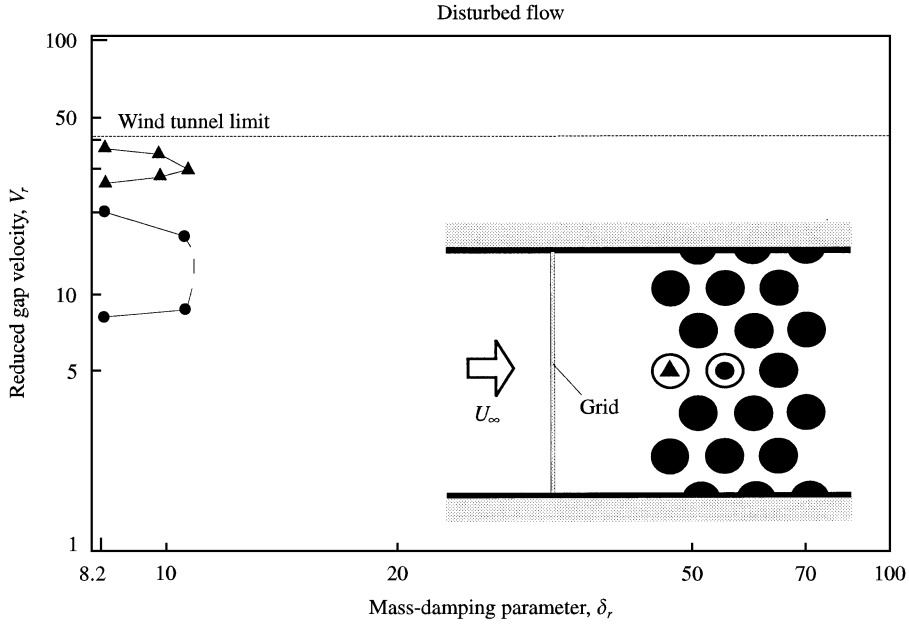

Figure 15. Stability diagram for one flexibly mounted tube in an otherwise fixed rotated triangular array ($P/d = 1{\cdot}375$) with increased turbulence (Tu = 10·1, $L_{x,\mathrm{red}} = 0{\cdot}29$).

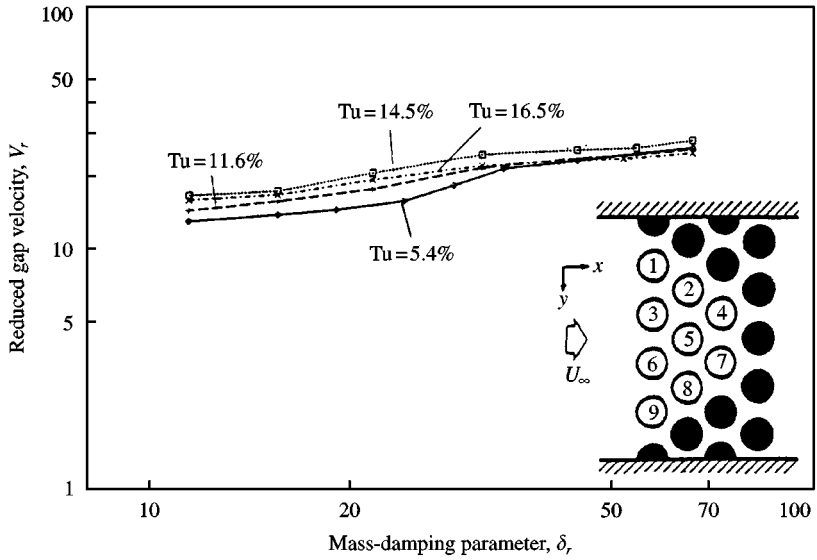

Figure 16. Stability diagram of a fully flexible tube bundle for a normal triangular array ($P/d = 1{\cdot}25$) with various turbulence intensities at the bundle inlet.

5. CONCLUSIONS

The investigations described in this paper were motivated by the fact that a flow disturbance *inside* the tube array (e.g., by trip-wires) can change the stability behaviour of *a single flexibly mounted tube* in the first few rows of an otherwise fixed array (Romberg & Popp 1996). Thus, the underlying question for the present study is the influence of a flow disturbance by means of increased turbulence already occurring *upstream* (at the inlet) of the array. The investigation holds for the first few tube rows, where the self-induced turbulence in the bundle is not fully developed. The present experimental study shows that upstream isotropic turbulence has a significant influence on the stability behaviour of a single flexibly mounted tube in an otherwise fixed array, where the fluid-damping-controlled instability (galloping) is the dominant excitation mechanism. Using different turbulence grids and distances it was possible to vary the turbulence intensity Tu and the length scale L_x of the upstream air-flow. The results of stability measurements with increased turbulence intensity Tu at the inlet of rotated and normal triangular arrays are different, depending on the array configuration.

(i) *Rotated triangular array* (a single flexible tube). Turbulence intensities from Tu = 3·5% to Tu = 23% and reduced length scales from $L_{x,\mathrm{red}} = 0{\cdot}21$ to $L_{x,\mathrm{red}} = 0{\cdot}39$ at the inlet of the array have been generated. With respect to the stability behaviour for the first four rows, a stabilization at increased turbulence has been found.

(ii) *Normal triangular array* (fully flexible bundle). Turbulence intensities from Tu = 5·4% to Tu = 21% and reduced length scales from $L_{x,\mathrm{red}} = 0{\cdot}24$ to $L_{x,\mathrm{red}} = 0{\cdot}38$ at the inlet of the array have been generated in this case. For this tube configuration an increasing turbulence has only a negligible influence on stability. The reasons for the different effects depending on the array configuration could be (a) a different dominant excitation mechanism, (b) different levels of self-induced turbulence, (c) different spatial correlations of the fluid forces. With respect to the important last two items, further experimental investigations are necessary.

ACKNOWLEDGEMENT

The authors gratefully acknowledge the financial support of this research work by the DFG (Deutsche Forschungsgemeinschaft, contract number Po 136/17/1).

References

Andjelić, M. & Popp, K. 1989 Stability effects in a normal triangular cylinder array. *Journal of Fluids and Structures* **3,** 165–185.

Austermann, R. & Popp, K. 1995 Stability behaviour of a single flexible cylinder in rigid tube arrays of different geometry subjected to cross-flow. *Journal of Fluids and Structure* **9,** 303–322.

Baines, W. D. & Peterson, E. G. 1951 An investigation of flow through screens. *Transactions of the ASME* **73,** 467– 480.

Batchelor, G. K. 1953 *The Theory of Homogeneous Turbulence*. Cambridge: Cambridge University Press.

Chen, S. S. 1983 Instability mechanisms and stability criteria of a group of circular cylinders subjected to cross-flow. Part I: theory. *ASME Journal of Vibration, Acoustic Stress and Reliability in Design* **103,** 51– 58.

Chen, S. S. 1984 Guidelines for the instability flow velocity of tube arrays in crossflow. *Journal of Sound and Vibration* **93,** 439– 455.

Chen, S. S. 1988 Some issues concerning fluidelastic instability of a group of circular cylinders in crossflow. In *Proceedings of 1988 International Symposium on Flow-Induced Vibration and Noise*. Vol 3: *Flow Induced Vibration and Noise in Cylinder Arrays* (eds M. P. Païdoussis, S. S. Chen & M. D. Bernstein), pp. 1–24. New York: ASME.

Connors, H. J. 1970 Fluidelastic vibration of tube arrays. In *Flow Induced Vibrations in Heat Exchangers* (ed. D. D. Reiff), pp. 42–56. New York: ASME.

Fage, A. & Warsap, J. 1929 The effects of turbulence and surface roughness on the drag of a circular cylinder. *Aeronautical Research Council R&M* No. 1283.

Frenkiel, F. N. 1948 The decay of isotropic turbulence. *Transactions of the ASME* **70,** 311–321.

Fung, Y. C. 1968 *The Theory of Aeroelasticity*. New York: Dover.

Gorman, D. J. 1979 The effect of artificially induced upstream turbulence on the liquid cross flow induced vibration of tube bundles. In *Flow-Induced Vibration of Power Plant Components* (ed. M. K. Au-Yang), Vol-PVP 41, pp. 33–43. New York: ASME.

Gross, H. G. 1975 Untersuchung aeroelastischer Schwingungsmechanismen und deren Berücksichtigung bei der Auslegung von Rohrbündelwärmetauschern. Ph. D. thesis, University of Hannover, Hannover, Germany (in German).

Lever, J. H. & Weaver, D. S. 1986 On the stability of heat exchanger tube bundles. Part I: modified theoretical model. *Journal of Sound and Vibration* **107,** 375–392.

Lindner, H. 1993 Untersuchungen zum Turbulenzeinfluss auf die Galloping–Schwingungen rechteckiger prismatischer Körper. Ph. D. thesis, University of Hannover, Hannover, Germany (in German).

Païdoussis, M. P., Price, S. J., Macdonald, R. & Mark, B. 1987 The flow-induced vibration of a single flexible cylinder in a rotated square array of rigid cylinders with pitch to diameter ratio of 2·12. *Journal of Fluids and Structures* **1,** 359–378.

Price, S. J. & Païdoussis, M. P. 1986 A constrained-mode analysis of the fluidelastic instability of a double row of flexible circular cylinders-subject to cross-flow: A theoretical investigation of system parameters. *Journal of Sound and Vibration* **105,** 121–142.

Rzentkowski, G. & Lever, J. H. 1995 An effect of turbulence on fluidelastic instability in tube bundles: a nonlinear analysis. In *Proceedings 6th International Conference on Flow Induced Vibration*, London (ed. P. W. Bearman), pp. 351–362. Rotterdam: A. A. Balkema.

Romberg, O. & Popp, K. 1996 The influence of trip-wires on the stability of tube bundles subjected to cross-flow. In *Proceedings of the ASME Pressure Vessels and Piping Conference*, Montreal, Canada, PVP-Vol. 328, pp. 3–10. New York: ASME. Also in *Journal of Fluids and Structures* (1998) **12,** 17–32.

Rotta, J. C. 1972 *Turbulente Ströemungen*. Stuttgart: B. G. Teubner (in German).

Sandifer, J. B. & Bailey, R. T. 1984 Turbulent buffeting of tube arrays in liquid crossflow. In *Proceedings Symposium on Flow-Induced Vibrations*, Vol. 2: Vibration of Arrays of Cylinders in Cross Flow (eds M.P. Païdoussis, M. K. Au-Yang & S. S. Chen, pp. 211–226. New York: ASME.

SOPER, B. M. H. 1982 The effect of grid generated turbulence on the fluidelastic instability of tube bundles in cross-flow. In *Heat Exchangers*: *Theory and Praxis* (eds Taborek, J., Hewitt, G. F., & Afgan, N.) pp. 325–337.

SOUTHWORTH, P. J. & ZDRAVKOVICH, M. M. 1975 Effect of grid turbulence on the fluidelastic vibrations of in-line tube banks in cross-flow. *Journal of Sound and Vibration* **39,** 461–469.

TAYLOR, G. 1938 Statistical theory of turbulence. In *Proceedings Royal Society of London* A **164,** 421–478.

WEAVER, D. S. & FITZPATRICK, J. A. 1987 A review of flow induced vibrations in heat exchangers. In *Proceedings BHRA Conference on Flow-Induced Vibrations* (ed. R. King), Bowness-on-Windermere, U.K., pp. 1–17.

APPENDIX: NOMENCLATURE

a	bar width of turbulence grid (mm)
s	mesh size of turbulence grid (mm)
b	distance between bundle inlet and bundle (m)
d	tube outside diameter, $d = 0{\cdot}08$ m
f_1	first natural tube frequency ($f_1 = 9.3$ Hz)
l	tube length, $l = 0{\cdot}8$ m
L	length scale (m)
L_x	length scale in x-direction (m)
$L_{x,\mathrm{red}}$	reduced length scale $L_{x,\mathrm{red}} = L/d$
P	tube pitch (m)
r	correlation width (m)
R	correlation function (m^2/s^2)
t	time (s)
Tu	turbulence intensity, $\mathrm{Tu} = \sigma_1/\overline{u_1}$ (%)
u	fluid velocity (m/s)
$\overline{u_1}$	mean value of u in in-flow direction (m/s)
U_∞	undisturbed upstream velocity $U_\infty = \overline{u_1}$ (m/s)
U	gap velocity (m/s)
V_r	reduced gap velocity, $V_r = U/(f_1 d)$
x	in-flow direction
X	grid distance (mm)
X_{red}	reduced grid distance, $X_{\mathrm{red}} = X/a$
y	cross-flow direction
α	relative angle of undisturbed flow (°)
δ	logarithmic decrement of damping
δ_r	mass-damping parameter, $\delta_r = \mu\delta/(\rho d^2)$
μ	tube mass per unit length, $\mu = 3{\cdot}04$ kg/m
ν	kinematic viscosity, $\nu = 0{\cdot}151\,\mathrm{cm}^2/\mathrm{s}$
ρ	fluid density, $\rho = 1{\cdot}197\,\mathrm{kg/m}^3$
σ_1	standard deviation of velocity fluctuation u_1 (m/s)
τ	correlation time (s)